Joint experimental and theoretical study on low-energy elastic electron scattering by gaseous alkynes: Differential cross sections, shape resonances, and methylation effects

M. A. Khakoo,[1] G. Tatreau,[1] J. G. Childers,[1] K. Oen,[2] J. Fernandez,[2] B. A. Hlousek,[1] M. Zawadzki,[3] F. P. Bardela,[4] L. V. S. Dalagnol,[5] G. M. Moreira,[5] M. H. F. Bettega,[5] and A. Souza Barbosa[5,*]

[1]*Department of Physics, California State University Fullerton, Fullerton, California 92831, USA*

[2]*Troy High School, 2200 Dorothy Lane, Fullerton, California 92831, USA*

[3]*Atomic Physics Division, Department of Atomic, Molecular, and Optical Physics, Faculty of Applied Physics and Mathematics, Gdańsk University of Technology, ul. G. Narutowicza 11/12, 80-233 Gdańsk, Poland*

[4]*Departamento de Quimíca, Universidade Federal de São Carlos, 13565-905 São Carlos, São Paulo, Brazil*

[5]*Departamento de Física, Universidade Federal do Paraná, Caixa Postal 19044, 81531-980, Curitiba, Paraná, Brazil*

(Received 27 February 2022; accepted 24 March 2022; published 19 April 2022)

A detailed comparison of experimental and theoretical elastic cross sections for low-energy electron scattering by ethyne (C_2H_2), taken earlier in our group by Gauf *et al.* [Phys. Rev. A **87**, 012710 (2013)], and some of its methylated derivatives, propyne (C_3H_4), and the isomers 1-butyne and 2-butyne (n-C_4H_6, $n = 1, 2$), taken here, are presented. The present differential cross sections were measured at incident electron energies ranging from 1 eV to 30 eV and for scattering angles from 5° to 130° using the relative flow method with an aperture gas source. Our earlier work was taken over a larger energy range of up to 100 eV. The theoretical calculations were carried out for impact energies up to 30 eV, employing the Schwinger multichannel method with pseudopotentials in the static-exchange plus polarization approximation. In addition to the differential cross sections, we present the integral and momentum transfer cross sections with which we discuss the shape resonances present in these systems and other physical phenomena, such as the presence of Ramsauer-Townsend minimum. We also compare our theoretical and experimental results with previous data that are available in the literature.

DOI: 10.1103/PhysRevA.105.042809

I. INTRODUCTION

Electron-molecule interaction plays a role in numerous areas of knowledge, from basic science to applications, including medicine, astronomy, and environmental sciences [1]. Some of the effects exploited in such studies include the methylation of molecules. For example, it is well known that methylation in DNA not only affects the interactions with other constituents, but is also closely related to some diseases, such as cancer, nervous system disorders, atherosclerosis, and cardiovascular disease [2–4]. Due to the inherent difficulties of working, both theoretically and experimentally, with molecules such as DNA, studies with small molecules, in particular hydrocarbons and their methylated derivatives, can reveal important properties related to the methylation effect. The importance of low-energy electron scattering from hydrocarbons has been highlighted previously, such as the work by Sanche and coworkers [5] on the fragmentation of DNA by low-energy dissociative electron attachment processes, and in fuels [6].

Alkynes are hydrocarbons that present a C ≡ C triple bond between carbon atoms and whose general chemical formula is $C_\nu H_{2\nu-2}$, for $\nu \geqslant 2$. The simplest alkyne, with $\nu = 2$, is ethyne, also known as acetylene (H − C ≡ C − H). Among the relatives in the alkyne family, we investigated electron scattering from propyne (methylacetylene, $H_3C - C \equiv CH$), which is a stable isomer of the C_3H_4 molecule, as well as two interesting stable isomers of C_4H_6, namely, 1-butyne (ethylacetylene, $C_2H_5 - C \equiv C - H$) and 2-butyne (dimethylacetylene, $CH_3 - C \equiv C - CH_3$). As is shown in Fig. 1, propyne and the C_4H_6 isomers can be seen as methylated versions of ethyne.

Also interesting are the markedly differing properties of the butyne isomers; while 1-butyne is nonsymmetric with a dipole moment of 0.80 D [7], 2-butyne is symmetric and has no dipole moment. Consequently, electron scattering from these species would reveal clear differences due to long-range dipole potential interaction as compared to short-range electron-atom or molecule interactions. This is likely to be seen at low incident electron energies and small scattering angles where polarization effects are prevalent over other interactions. While these isomers have no specific or significant industrial application, 1,2-butynes are used in specialty gas mixtures employed in the organic synthesis of compounds and instrument calibration. On combustion, 1-butyne releases carbon monoxide [8], and it is found in carbon-rich stars as a pathway for forming ethyne [9].

The study of low-energy electron collisions with these hydrocarbons has become a subject of interest that was investigated by several groups over the years. Here we will mention only the most recent ones. From the experimental point of view, Szmytkowski *et al.* [10], using the linear electron-transmission method, performed total cross-section (TCS) measurements for ethyne and 1-butyne at impact energies ranging from 0.5 to 300 eV. Additionally, Szmytkowski

*alessandra@fisica.ufpr.br

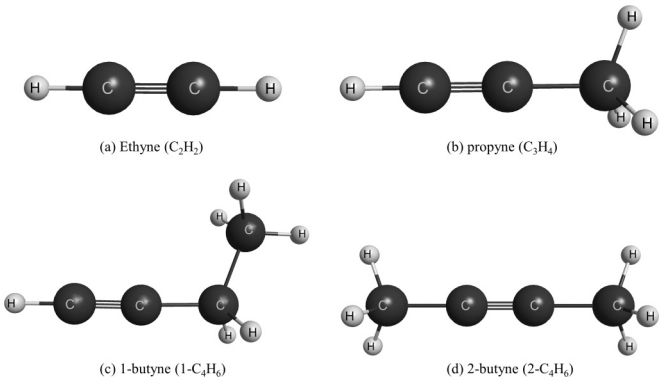

FIG. 1. Geometric structures of (a) ethyne, (b) propyne, (c) 1-butyne, and (d) 2-butyne. Figures obtained with the graphical interface MacMolPlt [47].

and Kwitnewski reported the TCS from 0.5 to 370 eV for propyne [11] and 2-butyne [12]. For propyne, there are TCS data by Makochekanwa *et al.* [13] in the energy range from 0.8 to 600 eV using the linear electron transmission method and differential cross sections (DCSs) measured by Nakano *et al.* [14]. From our group, Gauf *et al.* [15] measured DCSs for low-energy electron scattering from ethyne and compared the results with existing measurements of both total and differential cross sections for this target and with theoretical modeling. From the theoretical side Vinodkumar *et al.* [16] reported TCS for ethyne calculated using the R-matrix method. Lopes *et al.* calculated integral, differential, and momentum transfer cross sections for C_4H_6 isomers, among them being 2-butyne [17], and for propyne [18] using the Schwinger multichannel method at static-exchange approach. In 2005, Sanchez *et al.* discussed the polarization effects on electron scattering by C_3H_4 isomers, including propyne [19]. To the best of our knowledge, there are no theoretical cross section results for 1-butyne available in the literature.

Due to the paucity of cross section measurements and scattering calculations for butyne and a further interest in investigating both the isomer effect in 1,2-butynes and methylation effects in these alkynes, the present work is a joint theoretical and experimental study on electron scattering by ethyne, propyne, 1-butyne, and 2-butyne. The present measurements were taken at incident electron energies (E_0) of 1 eV to 30 eV and electron scattering angles (θ) of 10° to 130°. The calculations were carried out for impact energies up to 30 eV, using the well-established Schwinger multichannel method.

The remainder of this paper is as follows. In the next section we discuss pertinent aspects of the experimental and theoretical methods used, in Sec. III our results are presented and discussed, and finally we close this work with a summary of our findings in Sec. IV.

II. EXPERIMENTAL AND THEORETICAL PROCEDURES

A. Experimental method

The present experimental setup has been detailed before and was well tested, see, e.g., Ref. [20]. The electron gun and detector were made of titanium, employed double hemispherical energy selectors with cylindrical lenses, and was baked to approximately 100° C using magnetically free biaxial heaters [21]. Electrons were detected by a discrete dynode electron multiplier [22]. The remnant magnetic field in the collision region was reduced to ≈1 mG by a double μ-metal shield. Incident electron currents used were around 18–24 nA, with an energy resolution of between 40–60 meV, full-width at half-maximum. To counter space charge broadening of the incident electron beam lower currents were chosen at lower E_0 values. The electron beam remained stable, with the current varying less than 15% at maximum during the data acquisition period. The energy of the beam was established by observing the elastic scattering 2 ^{2}S He$^-$ resonance at 19.366 eV [23] at $\theta = 90°$ to about ≈40 meV stability during a daily run; typically the contact potential varied from 0.65 eV to 0.8 eV. Energy loss spectra of the elastic peak were collected at fixed E_0 and θ values by repetitive, multichannel-scaling techniques.

The effusive target gas beam was formed by flowing gas through a carbon-sooted 0.4-mm diameter and 0.03-mm-thick aperture collimator. Using an aperture source instead of a conventional tube gas collimator obviates the experimental need to maintain the gas pressures of the target gases in an inverse ratio of their molecular diameters, and thus removes an additional source of error that might occur in using tube collimators or similar, see, e.g., Ref. [24]. This is a great advantage since the setting and settling of drive pressures in the source drive is expedited in the application of the relative flow method, and the flow rates of the gases could be determined even if the drive pressures were varying during the course of the experiment [24], as is the case for many liquid polyatomic targets used in gaseous electron collision experiments. The aperture, located ≈6–7 mm below the axis of the electron beam, was incorporated into a movable source [24,25] arrangement. The movable gas source method determines background electron-gas scattering rates expediently and accurately [25].

The resultant propyne, 1-butyne, and 2-butyne DCSs were normalized using the relative flow method with helium as the reference gas, using DCSs from the established work of Nesbet [26] for $E_0 < 20$ eV and of Register *et al.* [27] for $E_0 \geqslant 20$ eV. Samples for the alkynes were obtained from Sigma-Aldrich^{TM} and were of $\geqslant$ 98.7% purity. Typical pressures behind the aperture ranged from 1.2 to 2 Torr for He. Similarly these pressures were 0.2 to 0.35 Torr for ethyne [15], 0.1 to 0.15 Torr for propyne, and 0.07 to 0.15 Torr for 1-, 2-butyne, resulting in a chamber pressure ranging from 1.0×10^{-6} Torr to 2×10^{-6} Torr. To prevent condensation in the gas bleed valve (Granville-Phillips Series 203 [28]) the copper gas source lines were baked at a temperature of about 80–90° C with the valves baked at a temperature of ≈70° C.

Each DCS was taken a minimum of two times to check reproducibility and weighted averaging was made of multiple data sets to obtain the final DCSs at each incident electron energy. Integral cross sections (ICS) and momentum transfer cross sections (MTCS) were evaluated from the measured DCS by extrapolating the DCS to $\theta = 0°$ and 180° as described in Ref. [29] and numerically integrating the extrapolations using a spline fit.

TABLE I. Present experimental DCS, ICS, and MTCS values for elastic electron scattering from propyne, for 1.0 up to 30.0 eV, with one standard deviation errors. Units are in 10^{-16} cm^{2}sr^{-1} for DCS and 10^{-16} cm^2 for ICS and MTCS.

$E_0 \longrightarrow$																				
θ(deg) $\downarrow$	1.0 eV		2.0 eV		3.0 eV		3.2 eV		5.0 eV		8.0 eV		10.0 eV		15.0 eV		20.0 eV		30.0 eV	
10																	44.0	6.0	53.0	7.6
15											16.7	2.2	18.5	2.6	25.8	3.4	28.8	3.8	30.7	3.9
20	5.52	1.10	4.89	0.68	12.5	1.5	14.1	2.1	10.3	1.3	13.2	1.7	14.7	1.8	18.8	2.4	18.4	2.3	17.0	2.1
25	4.13	0.53	3.52	0.39	8.54	1.04	9.29	1.26	8.77	1.05	11.5	1.4	11.5	1.4	13.5	1.7	12.7	1.5	9.20	1.19
30	2.74	0.39	2.86	0.33	6.00	0.70	7.68	0.96	7.00	0.87	8.87	1.10	8.59	1.04	10.2	1.3	7.90	0.98	5.30	0.64
40	2.24	0.33	2.21	0.25	4.48	0.55	5.22	0.67	5.69	0.69	5.66	0.71	5.56	0.69	5.63	0.66	4.27	0.54	2.52	0.31
50	1.78	0.28	2.17	0.25	3.28	0.38	4.48	0.55	4.39	0.54	3.86	0.48	3.32	0.42	3.32	0.44	2.36	0.30	1.59	0.20
60	1.81	0.22	2.76	0.31	3.44	0.40	3.97	0.49	3.26	0.38	2.68	0.34	2.48	0.30	2.48	0.27	1.38	0.17	1.01	0.13
70	1.69	0.24	2.93	0.34	3.01	0.36	3.92	0.50	2.80	0.35	2.35	0.29	1.99	0.25	1.99	0.20	1.04	0.13	0.560	0.068
80	1.26	0.22	2.70	0.33	2.33	0.27	3.52	0.43	2.32	0.28	2.14	0.24	1.68	0.22	1.68	0.18	0.913	0.113	0.471	0.058
90	1.02	0.16	2.11	0.25	2.06	0.24	2.08	0.25	2.02	0.26	2.06	0.24	1.41	0.18	1.41	0.15	0.750	0.092	0.429	0.055
100	1.11	0.12	1.60	0.18	1.88	0.17	1.62	0.21	1.87	0.24	1.77	0.20	1.14	0.14	1.14	0.15	0.795	0.098	0.391	0.047
110	1.11	0.14	1.57	0.18	1.47	0.03	1.62	0.19	1.53	0.19	1.56	0.18	1.08	0.13	1.08	0.15	0.702	0.088	0.430	0.055
120	1.04	0.13	1.18	0.14	1.49	0.17	1.59	0.21	1.45	0.18	1.32	0.16	1.14	0.14	1.14	0.15	0.751	0.096	0.729	0.094
130	1.28	0.17	0.865	0.11	1.51	0.18	2.16	0.28	1.44	0.18	1.49	0.19	1.34	0.17	1.34	0.18	0.906	0.112	0.993	0.130
ICS	24.8	3.9	25.7	3.0	39.1	5.0	49.6	7.4	38.1	4.8	40.6	5.0	37.7	4.9	41.8	5.3	36.3	4.8	32.2	4.5
MTCS	20.3	3.6	18.1	2.3	25.0	3.0	36.6	6.6	24.2	3.0	25.0	3.2	21.9	3.2	21.3	2.8	15.1	2.4	13.1	2.5

B. Theoretical method

The elastic electron-molecule scattering calculations were computed with the Schwinger multichannel (SMC) method [30] implemented with pseudopotentials [31] of Bachelet, Hamann, and Schlüter [32]. The details of the method are discussed in Refs. [30,31,33], so here we focus on the description of the essential aspects concerning the present calculations.

In the SMC method, the scattering amplitude is written as

$$f^{\mathrm{SMC}}(\vec{k}_f, \vec{k}_i) = -\frac{1}{2\pi} \sum_{m,n} \langle S_{\vec{k}_f} | V | \chi_m \rangle (d^{-1})_{mn} \langle \chi_n | V | S_{\vec{k}_i} \rangle, \quad (1)$$

such that

$$d_{mn} = \langle \chi_m | A^{(+)} | \chi_n \rangle, \quad (2)$$

and

$$A^{(+)} = \frac{1}{2}(PV + VP) - VG_P^{(+)}V + \frac{\hat{H}}{N+1} - \frac{1}{2}(\hat{H}P + P\hat{H}). \quad (3)$$

In the above equations, $\{|\chi_m\rangle\}$ is a set of $(N+1)$-particle configuration state functions (CSFs) used in the expansion of the trial scattering wave function, P is a projector onto the energy-allowed target electronic channels, $G_P^{(+)}$ is the free-particle Green's function projected onto the P space, V is the

TABLE II. Present experimental DCS, ICS, and MTCS values for elastic electron scattering from 1-butyne, for 1.0 up to 30.0 eV, with one standard deviation errors. Units are in 10^{-16} cm^{2}sr^{-1} for DCS and 10^{-16} cm^2 for ICS and MTCS.

$E_0 \longrightarrow$																		
θ(deg) $\downarrow$	1.0 eV		2.0 eV		3.0 eV		5.0 eV		8.0 eV		10.0 eV		15.0 eV		20.0 eV		30.0 eV	
10																	47.2	6.4
15							13.3	1.8	15.8	2.2	15.7	2.1	17.0	2.3	23.8	3.3	25.3	3.4
20	3.99	0.59	3.93	0.54	6.94	0.92	9.40	1.24	11.9	1.6	11.1	1.5	10.1	1.3	12.3	1.6	11.9	1.6
25	3.46	0.47	2.96	0.39	5.22	0.68	7.26	0.96	8.44	1.10	7.27	0.97	6.60	0.81	7.15	0.90	6.26	0.83
30	3.04	0.40	2.23	0.30	4.09	0.51	5.78	0.70	5.78	0.70	5.60	0.71	4.09	0.50	4.48	0.56	3.45	0.46
40	2.62	0.35	1.88	0.23	3.26	0.39	4.26	0.52	3.16	0.38	2.91	0.36	2.49	0.30	2.48	0.31	1.85	0.24
50	2.58	0.34	2.18	0.27	3.19	0.38	3.32	0.41	2.58	0.32	2.30	0.28	1.93	0.23	1.61	0.20	1.30	0.17
60	2.69	0.35	2.35	0.30	2.94	0.35	2.89	0.35	2.49	0.29	2.01	0.25	1.36	0.16	1.17	0.14	0.708	0.093
70	2.85	0.38	2.33	0.30	2.39	0.28	2.44	0.28	2.04	0.23	1.62	0.20	1.02	0.12	0.843	0.097	0.539	0.071
80	3.16	0.42	2.11	0.26	1.87	0.21	2.15	0.25	1.75	0.20	1.34	0.17	0.932	0.106	0.682	0.079	0.435	0.057
90	3.20	0.43	1.66	0.21	1.73	0.20	1.87	0.21	1.39	0.16	1.07	0.13	0.759	0.088	0.596	0.067	0.390	0.051
100	3.07	0.43	1.28	0.16	1.71	0.20	1.67	0.19	1.35	0.15	1.14	0.14	0.790	0.092	0.635	0.072	0.382	0.050
110	2.96	0.45	1.06	0.13	1.72	0.20	1.63	0.19	1.53	0.17	1.14	0.14	0.798	0.093	0.635	0.071	0.394	0.052
120	2.83	0.45	0.971	0.122	1.73	0.20	1.71	0.19	1.78	0.20	1.34	0.16	0.867	0.102	0.764	0.086	0.517	0.068
125	2.63	0.40	0.961	0.120	1.73	0.20	1.80	0.21	1.87	0.21	1.39	0.16	0.944	0.111	0.813	0.092	0.567	0.075
130	2.59	0.42	0.951	0.119	1.86	0.22	1.85	0.23	2.00	0.23	1.43	0.17	1.02	0.12	0.862	0.097	0.617	0.082
ICS	104	17	21.9	3.0	32.4	4.4	36.5	4.9	35.3	4.8	29.7	4.0	25.5	3.4	28.0	3.8	25.4	3.4
MTCS	101	16	16.6	2.2	25.7	3.5	25.7	3.5	25.5	3.4	18.7	2.5	14.7	2.0	12.1	1.6	8.69	1.17

TABLE III. Present experimental DCS, ICS, and MTCS values for elastic electron scattering from 2-butyne, for 1.0 up to 30.0 eV, with one standard deviation errors. Units are in 10^{-16} cm^{2}sr^{-1} for DCS and 10^{-16} cm^2 for ICS and MTCS.

$E_0 \longrightarrow$																				
θ(deg) $\downarrow$	1.0 eV		2.0 eV		3.0 eV		3.56 eV		5.0 eV		6.75 eV		10.0 eV		15.0 eV		20.0 eV		30.0 eV	
10																			75.8	10.8
15									13.4	2.0	21.3	2.9	26.1	3.4	18.2	2.4	27.5	3.9	29.6	4.1
20	1.83	0.25	1.94	0.26	4.89	0.66	9.71	1.54	10.3	1.4	15.9	2.1	18.3	2.3	13.3	1.8	14.2	1.9	15.5	2.1
25	1.55	0.20	1.68	0.20	4.21	0.52	6.54	0.80	8.46	1.00	11.8	1.4	12.5	1.5	10.0	1.2	9.27	1.13	9.27	1.18
30	1.33	0.17	1.67	0.20	3.50	0.43	5.18	0.64	7.05	0.83	9.19	1.10	9.81	1.19	6.70	1.21	6.73	0.81	5.95	0.76
40	1.17	0.14	2.06	0.24	3.41	0.40	4.38	0.52	5.62	0.67	6.22	0.74	5.90	0.72	4.33	0.80	3.48	0.42	2.26	0.28
50	1.24	0.15	2.34	0.28	3.44	0.42	3.76	0.46	4.52	0.54	4.47	0.53	3.74	0.46	2.46	0.51	1.57	0.19	1.37	0.17
60	1.41	0.17	2.34	0.28	3.04	0.37	2.97	0.36	3.74	0.45	3.38	0.41	2.51	0.31	1.58	0.29	1.32	0.16	0.937	0.117
70	1.59	0.20	2.12	0.25	2.46	0.30	2.38	0.29	3.16	0.38	2.87	0.35	1.94	0.24	1.50	0.19	1.07	0.13	0.609	0.076
80	1.60	0.20	1.67	0.21	2.10	0.26	2.12	0.27	2.64	0.32	2.62	0.32	1.64	0.20	1.32	0.18	0.901	0.114	0.466	0.059
90	1.51	0.18	1.22	0.15	1.76	0.21	1.83	0.22	2.10	0.25	2.38	0.29	1.38	0.17	0.983	0.121	0.701	0.084	0.363	0.045
100	1.23	0.15	0.861	0.106	1.53	0.19	1.70	0.21	1.75	0.21	1.92	0.24	1.22	0.15	0.882	0.108	0.701	0.085	0.398	0.050
110	1.08	0.15	0.647	0.080	1.28	0.15	1.48	0.18	1.57	0.19	1.76	0.21	1.23	0.15	0.983	0.117	0.752	0.089	0.458	0.057
120	0.980	0.139	0.502	0.062	1.04	0.13	1.35	0.16	1.67	0.20	1.86	0.22	1.18	0.14	1.18	0.14	0.874	0.103	0.612	0.076
130	0.911	0.131	0.455	0.057	0.972	0.118	1.34	0.16	2.03	0.24	2.31	0.27	1.65	0.20	1.41	0.17	0.837	0.097	0.758	0.095
ICS	15.9	2.3	16.7	2.4	26.8	3.8	34.7	5.0	44.0	6.1	51.4	7.2	46.9	6.6	35.3	5.0	33.2	4.7	36.2	5.2
MTCS	14.0	1.9	11.6	1.5	18.4	2.4	22.3	3.0	31.1	4.1	34.6	4.5	26.4	3.5	22.0	2.9	12.8	1.7	10.2	1.4

interaction potential, $\vec{k}_i$ ($\vec{k}_f$) is the incident (scattered) electron wave vector, $\hat{H} \equiv E - H$ is the collision energy minus the full Hamiltonian of the system ($H \equiv H_0 + V$), and $|S_{\vec{k}_{i,f}}\rangle$ is a solution of the unperturbed Hamiltonian H_0 represented by the product of a target state and a plane wave. The electronic cloud distortion due to the projectile field is accounted for through the virtual excitation of the target. This is included by performing calculations in the static-exchange plus polarization (SEP) approach, where the scattering wave function expanded in a trial basis set of CSFs is

$$|\Psi^{(+)}_{\vec{k}_i}\rangle = \sum_m c^{(+)}_{0m}|\chi_{0m}\rangle + \sum_{r>0}\sum_m c^{(+)}_{rm}|\chi_{rm}\rangle. \quad (4)$$

In Eq. (4) the first term corresponds to the static-exchange (SE) and the second to SEP. $c^{(+)}_{0m}(\vec{k}_i)$ and $c^{(+)}_{rm}(\vec{k}_i)$ are variational coefficients and $|\chi_{0m}\rangle$ and $|\chi_{rm}\rangle$ are the CSFs, which are given by

$$|\chi_{0m}\rangle = \mathcal{A}_{N+1}[|\Phi_0\rangle \otimes |\varphi_m\rangle], \quad (5)$$

$$|\chi_{rm}\rangle = \mathcal{A}_{N+1}[|\Phi_r\rangle \otimes |\varphi_m\rangle], \quad (6)$$

where $|\Phi_0\rangle$ is the target ground state obtained at the Hartree-Fock level, $|\varphi_m\rangle$ is a scattering orbital, $|\Phi_r\rangle$ are N-electron Slater determinants obtained by performing virtual excitations of the target, and $\mathcal{A}_{N+1}$ is the antisymmetrization operator.

Our calculations were carried out at the equilibrium geometry obtained at the second-order Møller Plesset perturbation theory level with a 6–31 G(1d) basis set using the GAMESS package [34]. The Cartesian Gaussian functions used for the carbon atoms were 5s5p3d functions and are described elsewhere [35]. For the hydrogen atoms, we employed the 4s/3s1p basis set of Dunning [36] with an additional p-function with exponent 0.75. Additionally, for the ethyne molecule we performed calculations employing extra centers (EC), following a similar procedure as employed by Bettega *et al.* for N_2O [37]. To account for the polarization effects improved virtual orbitals (IVOs) [38] were employed to represent the particle and scattering orbitals. To select the orbitals employed in our calculations we use the following strategy: all valence occupied orbitals were employed as hole orbitals whereas the IVOs with energy lower than 1.2 hartree were used as particle and scattering orbitals. Thus we obtained a total of 30514 CSFs for ethyne, 15618 CSFs for propyne, 6101 CSFs for 1-butyne, and 22440 CSFs for 2-butyne.

Propyne and 1-butyne present a permanent dipole moment, calculated to be 0.83 D and 0.87 D, respectively, in very close agreement to the experimental measurements of 0.78 D [39] and 0.80 D [7], for propyne and 1-butyne, respectively. Thus, since in the SMC method, the collision process involving polar molecules has a more appropriate description in the region of the molecular target, precisely due to the use of integrable square Cartesian Gaussian functions, it is necessary to employ the Born-closure approach [40] to properly describe the long-range effects on the cross sections. In this approach the low partial waves are computed using the SMC method whereas the higher partial waves (for $\ell > \ell_{\rm SMC}$) are calculated employing the scattering amplitude of the dipole potential computed in the first Born approximation (FBA). The $\ell_{\rm SMC}$ values depend on the incident energy and are chosen to provide the best agreement between calculated DCSs obtained with and without the Born-closure correction at scattering angles above typically 30°. In the present calculations we choose, for propyne $\ell_{\rm SMC} = 3$ for impact energies up to 1.5 eV, $\ell_{\rm SMC} = 4$ at 2.0 and 2.5 eV, $\ell_{\rm SMC} = 5$ for energies between 3.0 and 4.5 eV, $\ell_{\rm SMC} = 6$ for 5.0–6.5 eV, $\ell_{\rm SMC} = 7$ for 7.0–9.0 eV, $\ell_{\rm SMC} = 8$ for 9.5–16 eV, $\ell_{\rm SMC} = 9$ for 17–30 eV. And for 1-butyne $\ell_{\rm SMC} = 1$ up to 10 are summarized as $\ell_{\rm SMC} = 1$ for 0.1–0.5 eV; $\ell_{\rm SMC} = 2$ for 0.6–0.8 eV; $\ell_{\rm SMC} = 3$ for 0.9 eV; $\ell_{\rm SMC} = 4$ for 1.0–1.9 eV; $\ell_{\rm SMC} = 6$ for 2.0–4.9 eV; $\ell_{\rm SMC} = 4$ for 5.0–9.5 eV; $\ell_{\rm SMC} = 6$ for 10.0–13.0 eV; $\ell_{\rm SMC} = 7$ for 14.0–16.0 eV; $\ell_{\rm SMC} = 8$ for 17.0–20.0 eV; $\ell_{\rm SMC} = 9$ for 22.5–25.0 eV; and $\ell_{\rm SMC} = 10$ for 27.5–30.0 eV.

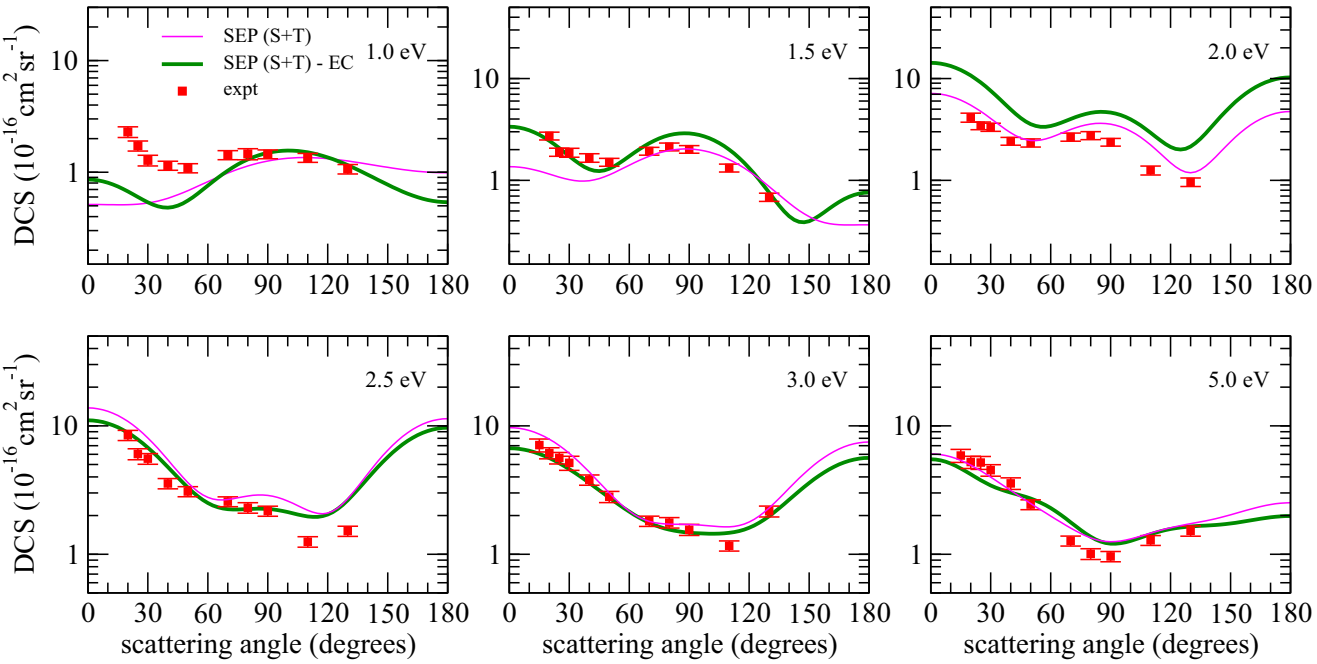

FIG. 2. Differential cross section for elastic scattering of electrons by ethyne at 1.0, 1.5, 2.0, 2.5, 3.0, and 5.0 eV. Calculations: green and magenta solid lines, obtained with and without extra centers. Red squares: previous measurements of Gauf *et al.* [15]. See text for the discussion.

III. RESULTS AND DISCUSSION

A. Differential cross sections

Tabulated values of experimental DCSs, ICSs, and MTCSs for ethyne are given in Ref. [15]. Similarly, the values of the present DCSs, ICSs, and MTCSs for propyne, 1-butyne, and 2-butyne are given in Tables I, II, and III, together with their uncertainties. Figures 2–7 show our calculated and measured differential cross sections for ethyne (Figs. 2 and 3), propyne (Fig. 4), 1-butyne (Fig. 5), and 2-butyne (Figs. 6 and 7) at selected energies. For ethyne, we also show in Figs. 2 and 3 our calculated results obtained employing extra centers, whereas in Fig. 4 for propyne and in Fig. 5 for 1-butyne, we show our corrected (SEP + Born) and uncorrected (SEP) calculated DCSs. In general, we observe overall good agreement between experiment and theory. We also show in Fig. 4 the previous measured data from Nakano *et al.* for propyne [14] and calculations results from Sanchez *et al.* for propyne [19].

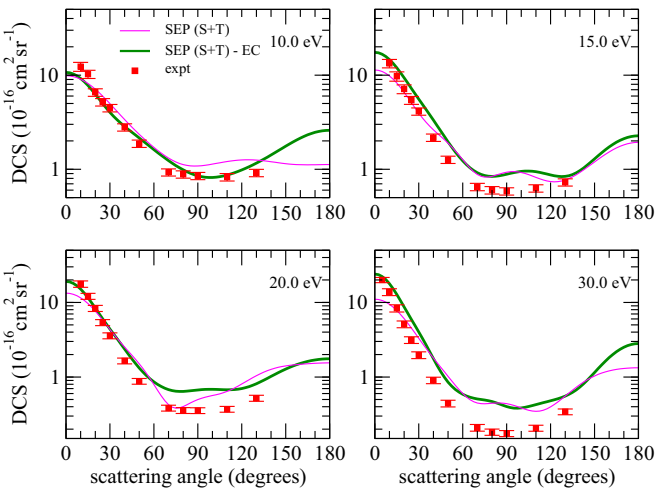

FIG. 3. Differential cross section for elastic scattering of electrons by ethyne at 10.0, 15.0, 20.0, and 30.0 eV. Green and magenta solid lines: present calculations obtained with and without extra centers. Red squares: Previous measurements of Gauf *et al.* [15]. See text for the discussion.

It is observed in Fig. 2 that the oscillatory behavior of the DCSs for ethyne at energies from 1.5–3.0 eV presents a d-wave pattern. This is probably due to the existence of shape resonances present in this energy range; this will be discussed later. Interestingly, in propyne, an ethyne methylated derivative, the oscillatory behavior of the DCSs at 3.0 eV, shown in Fig. 4, seems to have a contribution from an f wave. In the double methylated derivatives, 1- and 2-butyne, it is somewhat more difficult to identify the oscillatory behavior of the DCSs at these lower energies. This indicates that for these species different partial waves would seem to contribute.

Electron scattering by propyne was previously investigated with theoretical and experimental methods. The calculated results of Sanchez *et al.* [19] for propyne, obtained with the SMCPP method and the experimental data of Nakano *et al.* [14] are also shown in Fig. 4. In general, an overall good agreement between present and previous results is found. It is observed some small differences between both sets of calculations which are due to the different polarization schemes employed in each calculation.

At energies typically above 10.0 eV or 15.0 eV we observe differences in the magnitude of the DCSs between theory and experiment for all targets, the theory being larger than the experiment. This can be attributed to the theory lacking

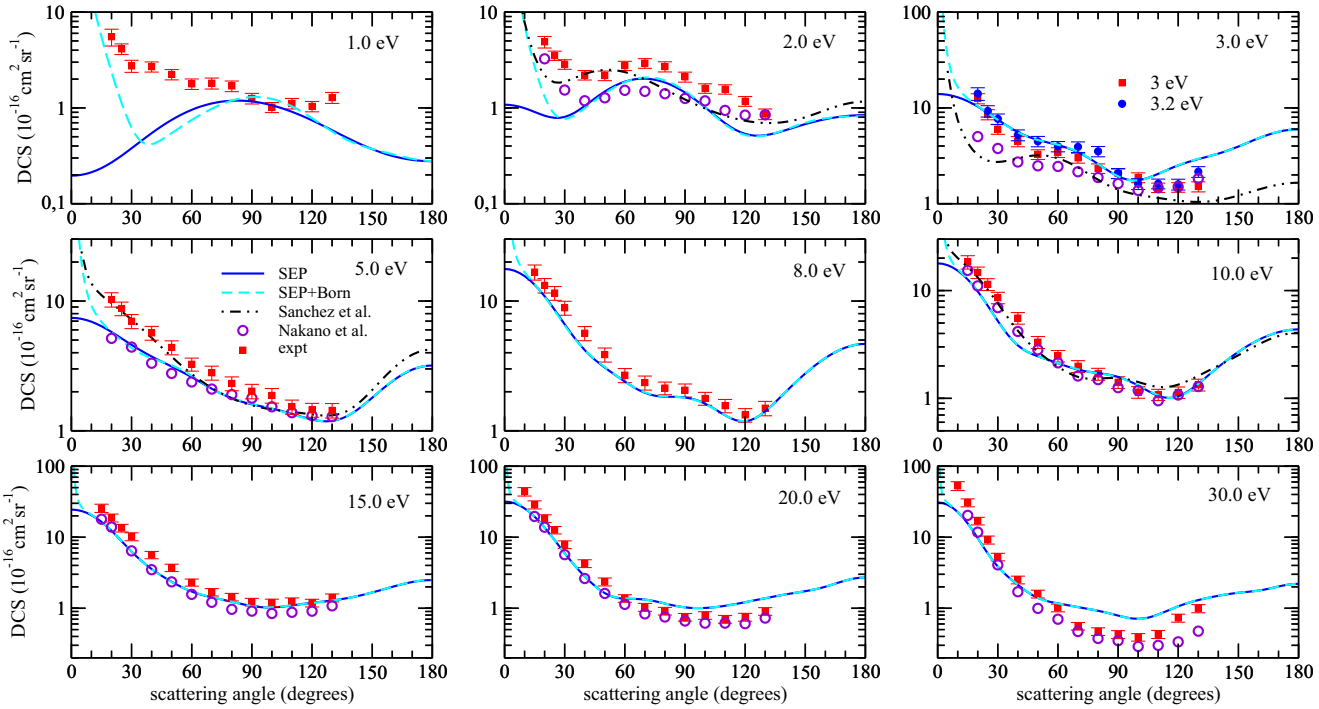

FIG. 4. Differential cross section for elastic scattering of electrons by propyne at 1.0, 2.0, 3.0, 5.0, 8.0, 10.0, 15.0, 20.0, and 30.0 eV. Dashed cyan and solid blue lines: present calculations obtained with and without Born-closure scheme. Dashed dotted black line, calculations of Sanchez *et al.* [19]. Violet circles: Experimental data from Nakano *et al.* [14]. Red squares: Present measurements. See text for the discussion.

the full inclusion of other open channels above the ionization energy (e.g., electronically excited states) that are treated as closed channels in our present calculations. Comparing the DCSs for 1-butyne (Fig. 5) and 2-butyne (Figs. 6 and 7) shows these targets to have very similar DCSs. The dipole-enhanced 1-butyne interaction does not produce a marked increase in

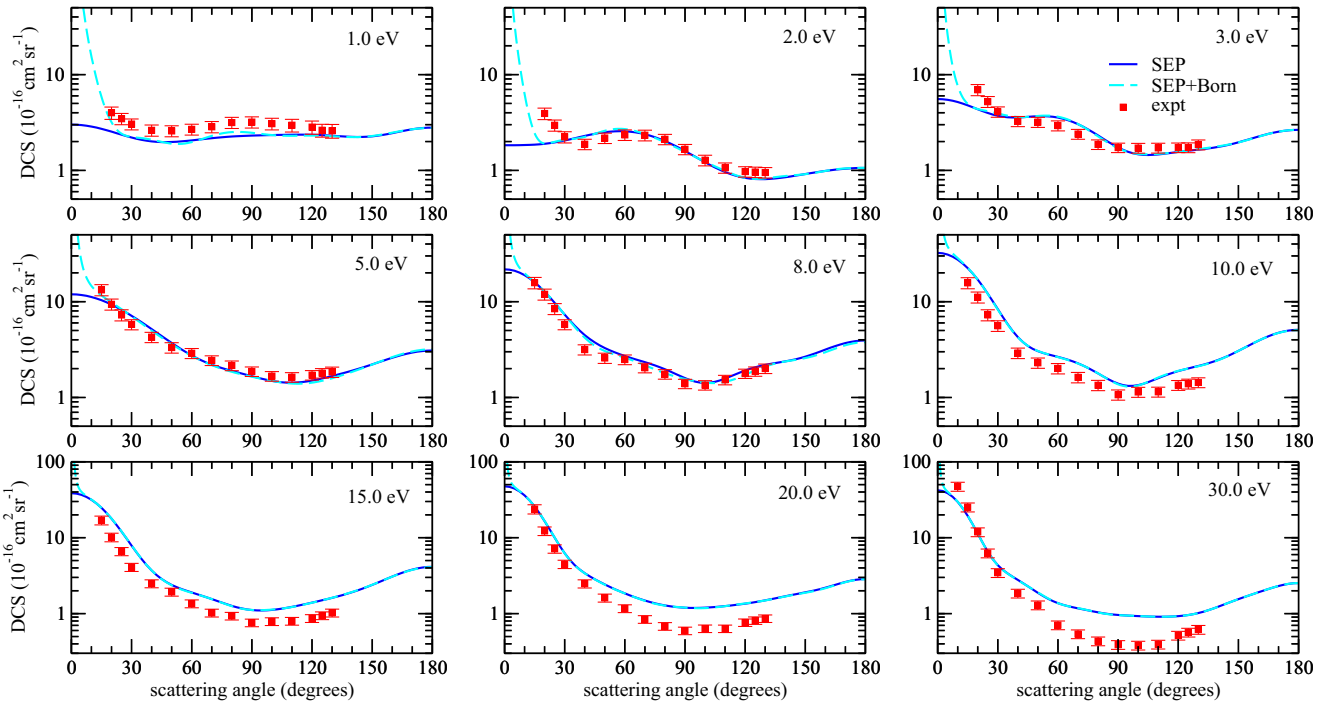

FIG. 5. Differential cross section for elastic scattering of electrons by 1-butyne at 1.0, 2.0, 3.0, 5.0, 8.0, 10.0, 15.0, 20.0, and 30.0 eV. Dashed cyan and solid blue lines: present calculations obtained with and without Born-closure scheme. Red squares: present measurements. See text for the discussion.

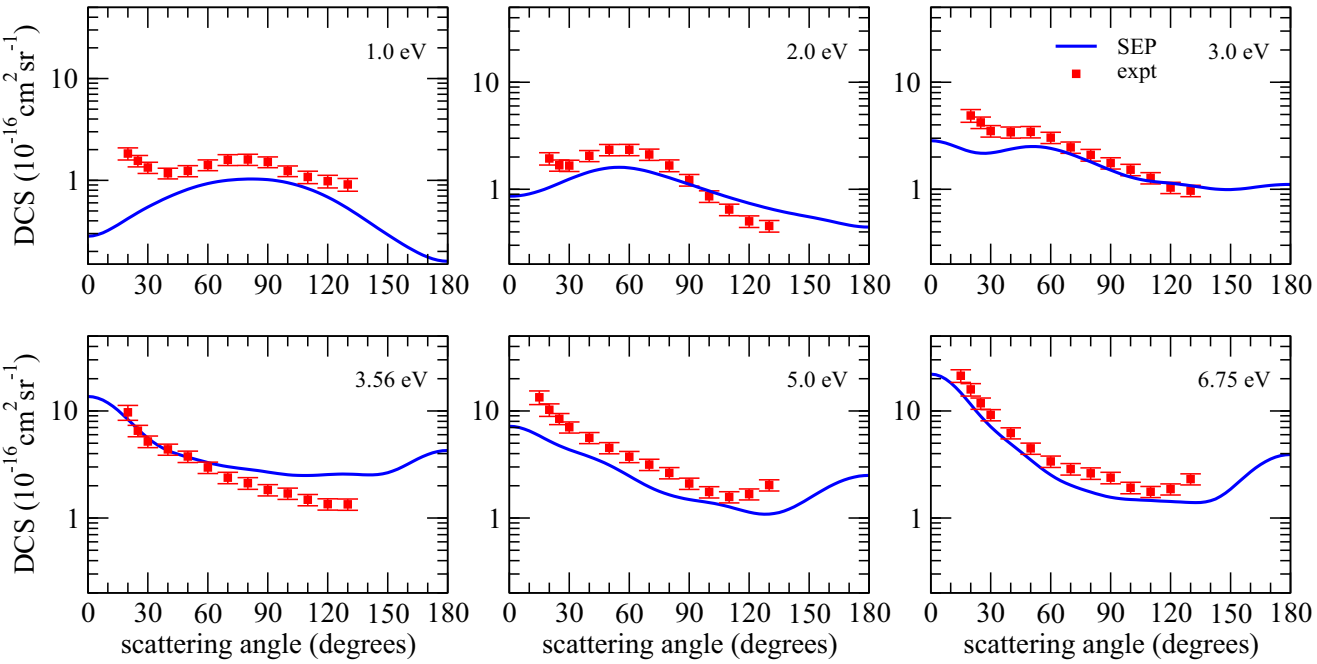

FIG. 6. Differential cross section for elastic scattering of electrons by 2-butyne at 1.0, 2.0, 3.0, 3.56, 5.0, and 6.75 eV. Solid blue line: present calculations; red squares: present measurements. See text for the discussion.

the DCSs at small scattering angles. This dipole moment of 0.8 D is small compared to other prevalent polyatomics such as water (1.88 D) [41]. However, at E_0 of 2.0 and 3.0 eV (Figs. 5 and 6) we note significant differences between these two targets for scattering angles below 50° where the long-range dipole interaction of 1-butyne results in clearly raised DCSs by as much as a factor of ≈3 over those of 2-butyne.

Comparing the DCSs of ethyne, propyne, and 1-, 2-butyne at an intermediate E_0 value of 10.0 eV or 15.0 eV from Figs. 3–5 7 shows the expected increased DCSs according to the mass of these targets. Whereas this increase is significant for ethyne to propyne, about ≈60%, it is only a ≈20% increase for propyne to either butyne. This consistency between our DCSs for the four targets presented here is encouraging.

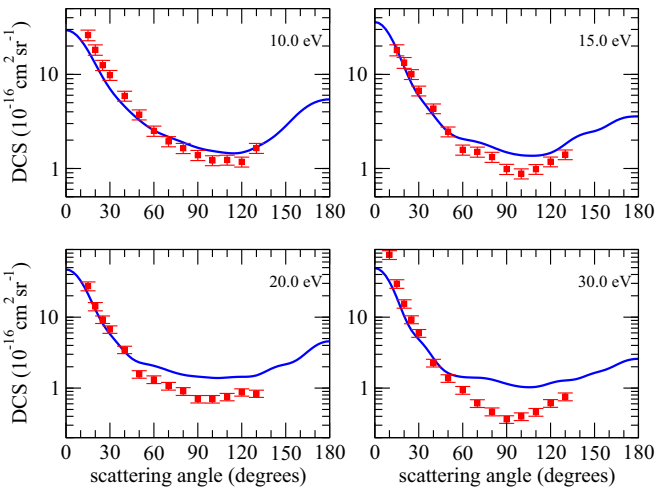

FIG. 7. Differential cross section for elastic scattering of electrons by 2-butyne at 10.0, 15.0, 20.0, and 30.0 eV. Solid blue line: present calculations; red squares: present measurements. See text for the discussion.

B. Integral and momentum transfer cross sections

Our integral and momentum transfer cross sections for ethyne are shown in Fig. 8. For comparison purposes, the calculated cross sections with and without the inclusion of extra centers (EC) are shown. We also compare our ICSs with the previous measurements of TCSs by Szmytkowski *et al.* [10], where we observe that good agreement is found between our TCSs and theirs. In both the theoretical and experimental results, we note a narrow structure peaked around 2.0–2.5 eV and, in the theoretical SEP($S+T$) and SEP($S+T$)-EC results, a broad feature at around 7.0 eV. A similar behavior is found in the Szmytkowski *et al.* TCSs [10]. A broad structure in the ICSs in the 5–10 eV E_0 range is characteristically found in cross sections for electron-hydrocarbon scattering and is well known to be due to the overlap of several σ^* shape resonances. The first structure, peaking at around 2.1 eV in the SEP($S+T$)-EC and at 2.5 eV in the SEP($S+T$) calculations is due to the capture of the incoming electron in a π^* orbital, forming a shape resonance. This is better discussed later.

It is also seen in Fig. 8 that the ICS (and MTCS) tend towards zero as the impact energy is decreased. To investigate this issue, we show in Fig. 9 the cross section for the A_g symmetry and its s-wave component in the upper panel, and the s-wave eigenphase is shown in lower panel. It is noted that the s-wave cross section (upper panel) shows a minimum located at 0.06 eV, the same energy where the s-wave eigenphase changes sign. This is the signature of a Ramsauer-Townsend minimum. For an attractive potential,

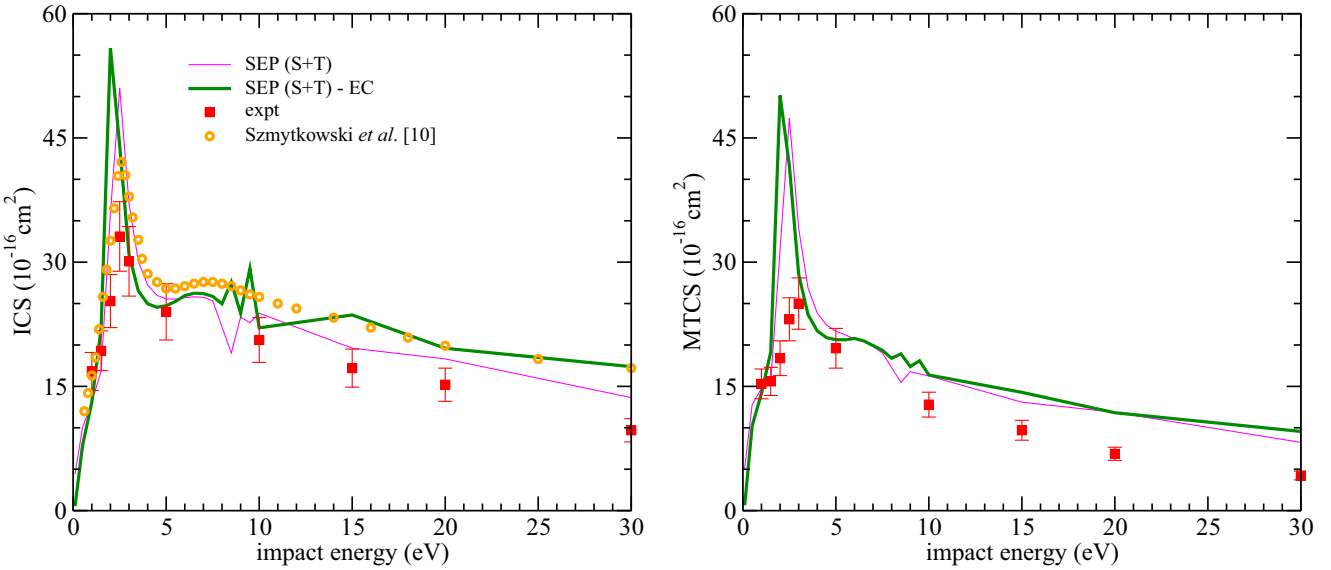

FIG. 8. Integral (left) and momentum transfer (right) cross sections for ethyne. Green and magenta solid lines: present calculations obtained with and without extra centers. Red squares: previous measurements of Gauf *et al.* [15]. Orange circles: total cross sections measurements by by Szmytkowski *et al.* [10].

the eigenphase is positive and for a repulsive potential it is negative. The sign change in the eigenphase indicates that the scattering potential changes from attractive to repulsive. In the SEP approach, the net scattering potential is given by attractive (static and polarization) and repulsive (exchange) potentials. As a consequence of the cancellation between the attractive and repulsive potentials, a minimum is observed in the cross section.

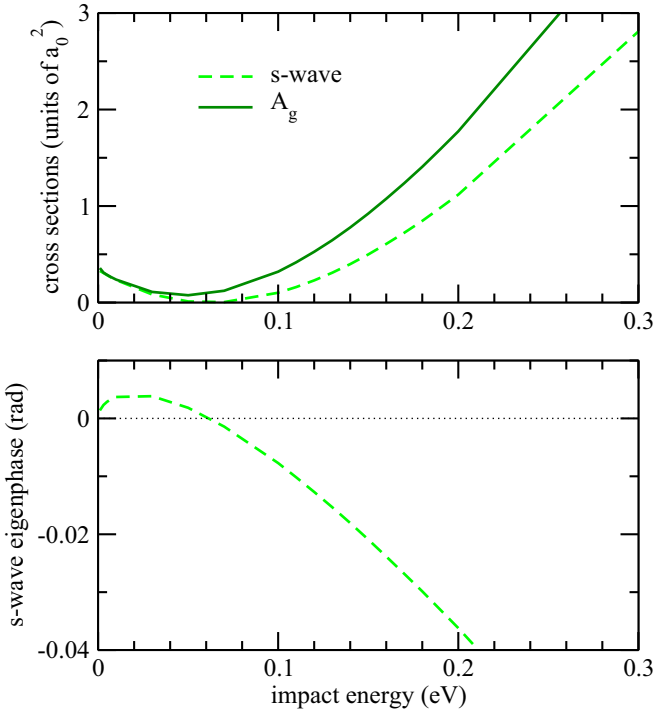

FIG. 9. *s*-wave cross section (upper panel) and corresponding *s*-wave eigenphase (lower panel). See text for discussion.

Our ICS and MTCS for propyne are displayed in Fig. 10 and compared with previous TCS data from Szmytkowski and Kwitnewski [11,13] and Makochekanwa *et al* [13]. Since propyne has a dipole moment we show our calculations both with (SEP + Born) and without (SEP) the Born-closure approach. It is seen that our experimental ICS, in general, have a larger magnitude than our calculations. Since our calculated and experimental MTCS are in good agreement, the difference in magnitude in our ICS is probably related to the extrapolation of the experimental DCSs at small scattering angles to perform the integration. The MTCS is obtained from the integration of the DCS weighted by the factor $(1 - \cos\theta)$, which significantly reduces the forward scattering contribution.

Figure 11 shows our calculated and experimental ICS and MTCS for 1-butyne compared with the measured TCS available in the literature [10]. Since 1-butyne also has a dipole moment, we show here our calculated results with and without the Born-closure approach. In our calculations, we observed a prominent structure centered at 3.5 eV and a second structure, which is a superposition of shape resonances of the form σ^* and background scattering at around 9.0 eV. In comparison with the present experimental data, it is seen that the overall behavior of the cross sections is quite similar although the magnitudes are somewhat different. In the previous section it was seen that the overall agreement between our calculated and experimental DCSs are very good; thus this difference in magnitude could be related to our extrapolations for the integration of the DCS at small scattering angles.

In Fig. 12 we compare our integral and momentum transfer cross sections for 2-butyne with the measured TCS from Szmytkowski and Kwitnewski [12]. It is worth mentioning some features observed in this figure: the cross sections decrease as the impact energy goes to zero and two prominent structures, one located at around 3.5 eV and another one near 8.5 eV.

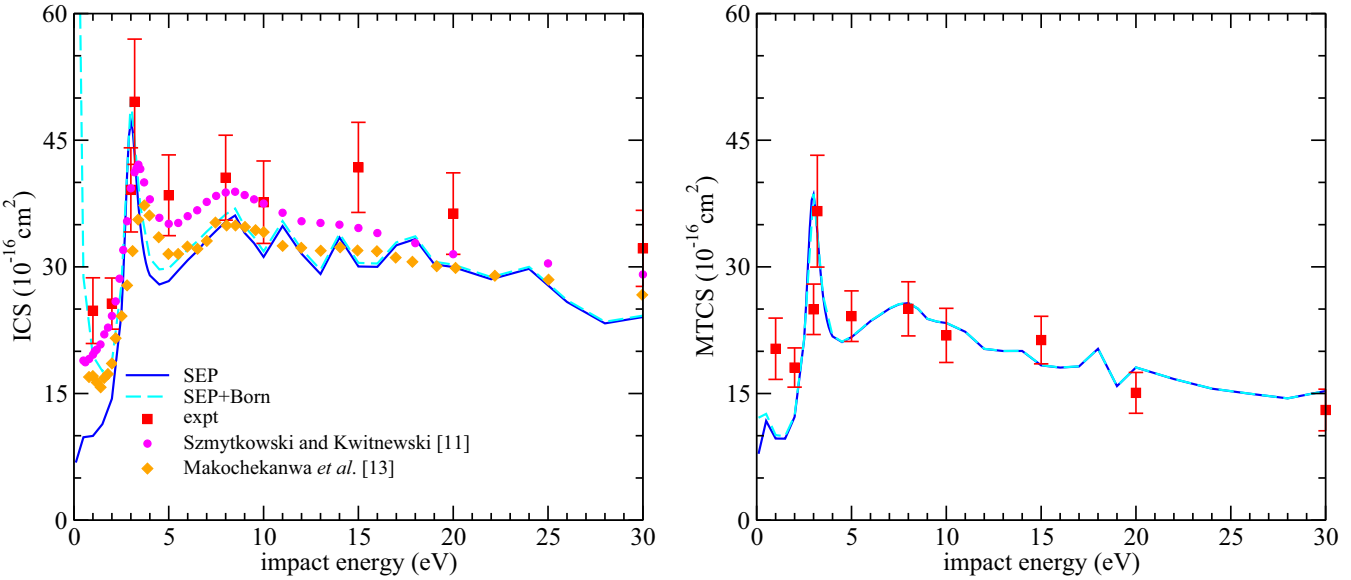

FIG. 10. Integral (left) and momentum transfer (right) cross sections for propyne. Dashed cyan and solid blue lines: present calculations obtained with and without Born-closure scheme. Red squares: present measurements. Magenta circles and orange diamonds: experimental TCS measured by Szmytkowski and Kwitnewski *et al.* [11] and by Makochekanwa *et al.* [13], respectively.

2-butyne is also an apolar molecule, thus the drop in the cross sections, as the impact energy goes toward zero, is indicative of the presence of a Ramsauer-Townsend minimum as was found for ethyne. Thus, we also present for 2-butyne, in Fig. 13, the cross section for the totally symmetric symmetry and its *s*-wave component (upper panel) and the respective *s*-wave eigenphase (lower panel). From this figure is observed that at 0.08 eV the signature of a Ramsauer-Townsend minimum occurs: the *s*-wave eigenphase crosses zero at the same energy where *s*-wave cross section vanishes.

Figures 11 and 12 also show the comparison of our present elastic integral cross sections and the previously measured total cross sections of Smytkowsky *et al.* [10,12], for 1- and 2-butyne, respectively. Regarding the structures present in both elastic and total cross sections it is seen that although the energy position of the first resonant structure are in good agreement, the position of the broader structure is poorly described. In fact, the experimental TCSs show this structure at around 7.5 eV for both conformers, while in our calculations these structures appear at around 9.5 eV and 8.5 eV, for 1- and 2-butyne, respectively. This difference is due to some lack in the polarization description for the broader structure. Although not shown here, our calculations are carried out for each irreducible representation of the molecular

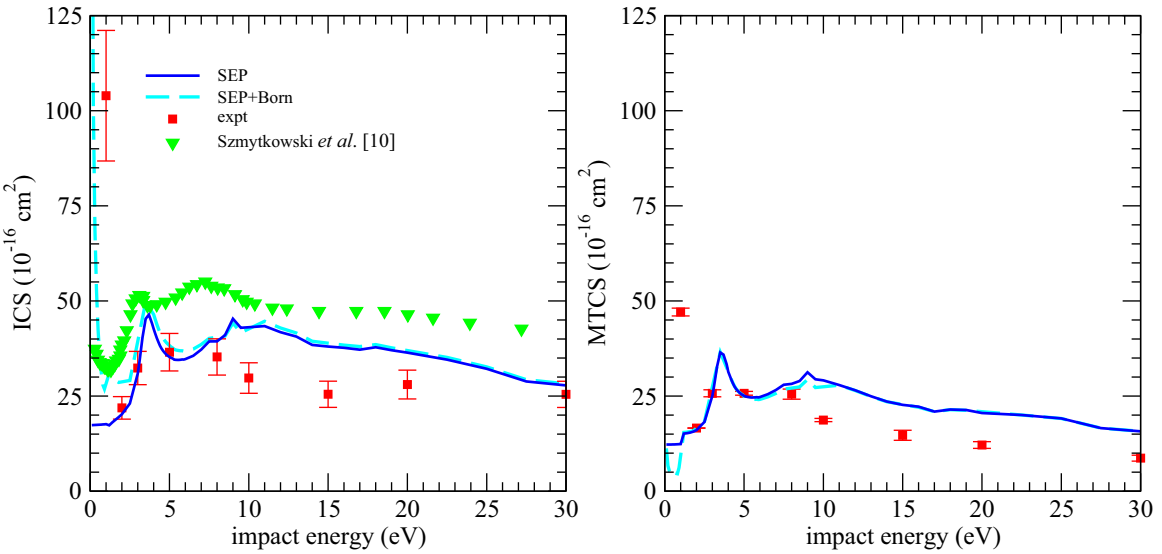

FIG. 11. Integral (left) and momentum transfer (right) cross sections for 1-butyne. Dashed cyan and solid blue lines: present calculations obtained with and without Born-closure scheme. Red squares: present measurements. Green triangles: experimental TCS by Szmytkowski *et al.* [10].

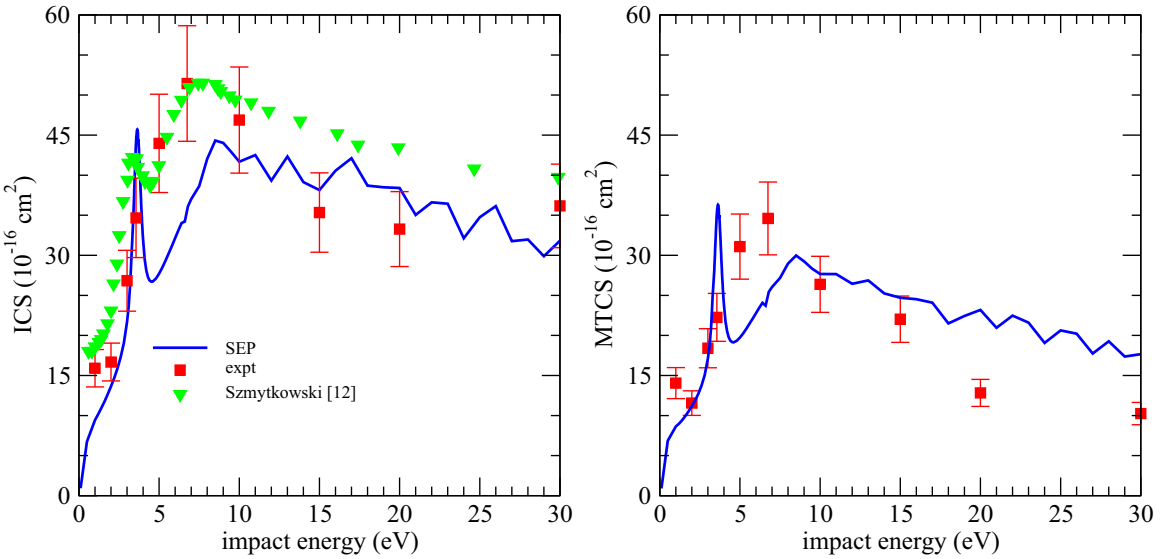

FIG. 12. Integral (left) and momentum transfer (right) cross sections for 2-butyne. Solid blue line: present calculations. Red squares: present measurements. Green triangles: experimental TCS by Szmytkowski *et al.* [12].

symmetry group. Since for both conformers the broader resonance structure appears in the same symmetry of the first resonance, it is difficult to balance the inclusion of polarization effects to describe correctly the higher-lying resonance and avoid overcorrelation of the low-lying resonance.

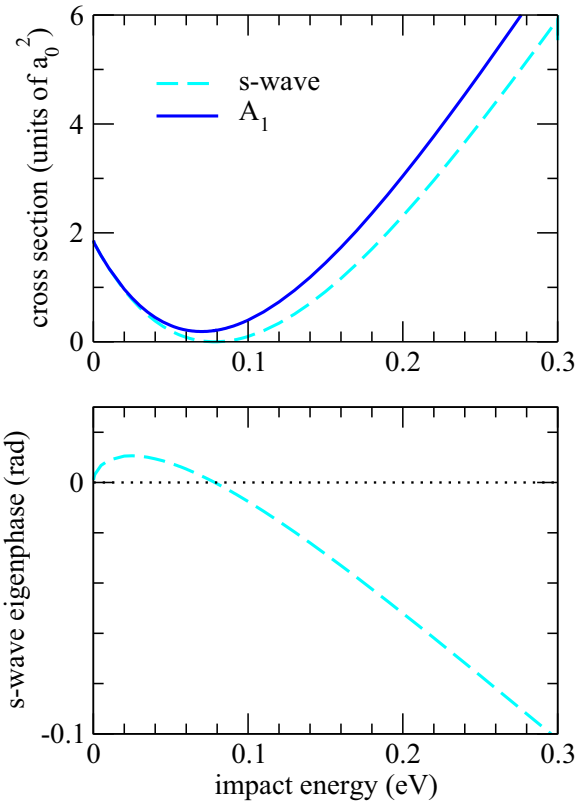

FIG. 13. *s*-wave cross section (upper panel) and its corresponding eigenphase (lower panel) for the 2-butyne molecule. See text for discussion.

Finally, in Fig. 14 we compare the calculated (left panel) and experimental (right panel) momentum transfer elastic cross sections for ethyne, propyne, 1-, and 2-butyne. We choose to show the MTCS for a fair comparison between the four targets since the weighting factor $(1 - \cos\theta)$ minimizes the effects of the dipole moment in the cross sections of propyne and 1-butyne. Such comparison is necessary to analyze how the methylation affects the ICS. The cross sections have a similar shape, however, they differ in magnitude. This can be clearly seen when comparing the cross section of ethyne and propyne, for example. The molecular size due the extra methyl group is the origin of the difference in the magnitude. This is similar when going from propyne to the butynes as was also observed in the overall comparisons of the DCSs.

C. Shape resonances

All of the ICS and MTCS presented above show a prominent and narrow structure at lower energies (between 2.0 and 4.0 eV). As mentioned before, this feature is related to the attachment of the incoming electron in a π^* orbital, characterizing a shape resonance. We summarize the resonance positions for all targets in Table IV, where we also show the estimated positions obtained with an empirical scaling relation [42] that relates the virtual orbital energy (VOE) to the vertical attachment energy (VAE). This relation is given by VAE $= 0.64795 \times$ VOE $- 1.4298$ (both VAE and VOE in eV).

The π^* resonance for ethyne is peaked at around 2.10 eV, in our calculations. This resonance is related to the attachment of the electron in the lowest unoccupied molecular orbital (LUMO), which presents a π^* character. Although ethyne belongs to the $D_{\infty h}$ point group, our calculations were performed in the abelian D_{2h} symmetry point group. Thus, the degenerate LUMO, which belongs to the Π_g symmetry of the $D_{\infty h}$ point group, is the

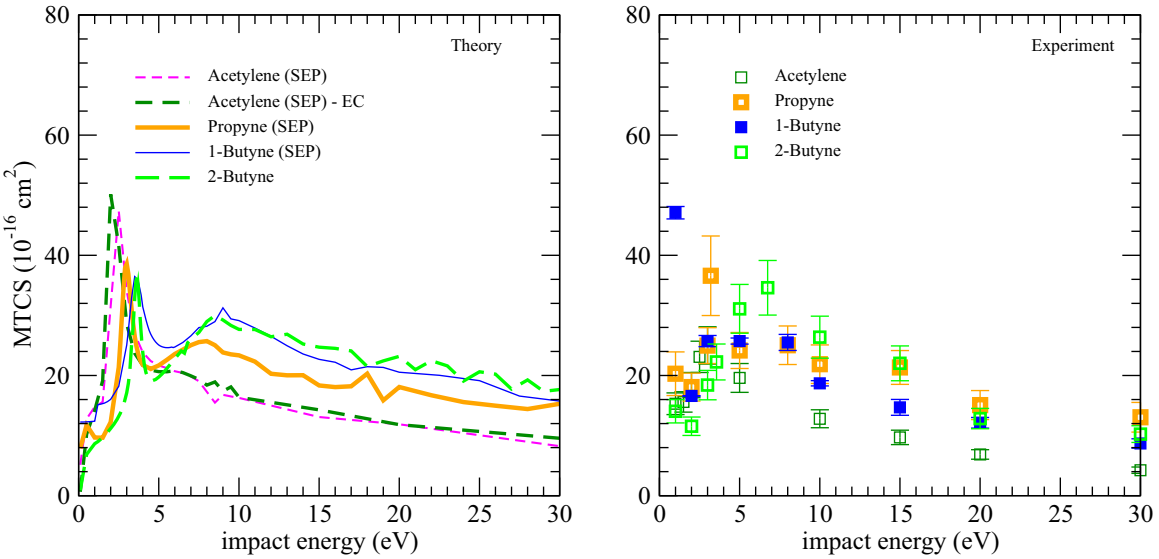

FIG. 14. Comparison among the present cross sections for electron collisions with ethyne, propyne, 1- and 2-butyne. In left panel we show the calculations at static exchange plus polarization approach and in right panel the experimental data. Olive dashed line and square: ethyne; orange solid line and square: propyne; blue thin solid line and solid square: 1-butyne; light green dashed line and squares: 2-butyne.

combination of the orbitals shown in Figs. 15(a) and 15(b), which belong to the B_{2g} and B_{3g} symmetries of the D_{2h} point group, respectively.

This first shape resonance in ethyne was previously studied by several experimental and theoretical methodologies (see, for instance, Ref. [44] and references therein), placing this resonance at energies between 1.7 and 2.6 eV. In particular, our calculated resonance energy position is in relatively good agreement with the value of 2.6 eV reported by the authors of Ref. [10] in their TCS data, and with earlier measurements, obtained through the trapped-electron technique, indicating this resonance at 1.7 eV [45] and 2.0 eV [46].

With our experimental apparatus, a way to corroborate the presence of shape resonances is to measure the differential cross sections at a fixed scattering angle (θ) as a function of the collision energy, the so-called excitation functions. In Fig. 16 we show our experimental and calculated excitation functions for all alkynes discussed in this work, obtained at $\theta = 90°$. In the case of ethyne, in Fig. 16(a), a very good agreement is found in the resonance position between theoretical and experimental data.

TABLE IV. Resonance positions, in eV, for the ethyne, propyne and 1-,2-butyne, obtained in the SEP approximation and experimental values available in the literature. For the sake of comparison, we also show the estimated vertical attachment energy (VAE) as obtained using a scaling relation.

Molecule	Character	SEP ($S+T$)	Experimental	VAE
Ethyne	π^*	2.10	2.6[a,b], 1.7[c], 2.0[d]	2.31
Propyne	π^*	3.00	3.4[a], 3.0[c], 2.8[d]	2.41
1-Butyne	π_1^*	3.50	3.2[a], 2.8[c], 2.4[d]	2.24
	π_2^*	3.70	–	2.43
2-Butyne	π^*	3.60	3.6[a], 3.6[c]	2.48

[a]Reference [10].
[b]Reference [43].
[c]Reference [45].
[d]Reference [46].

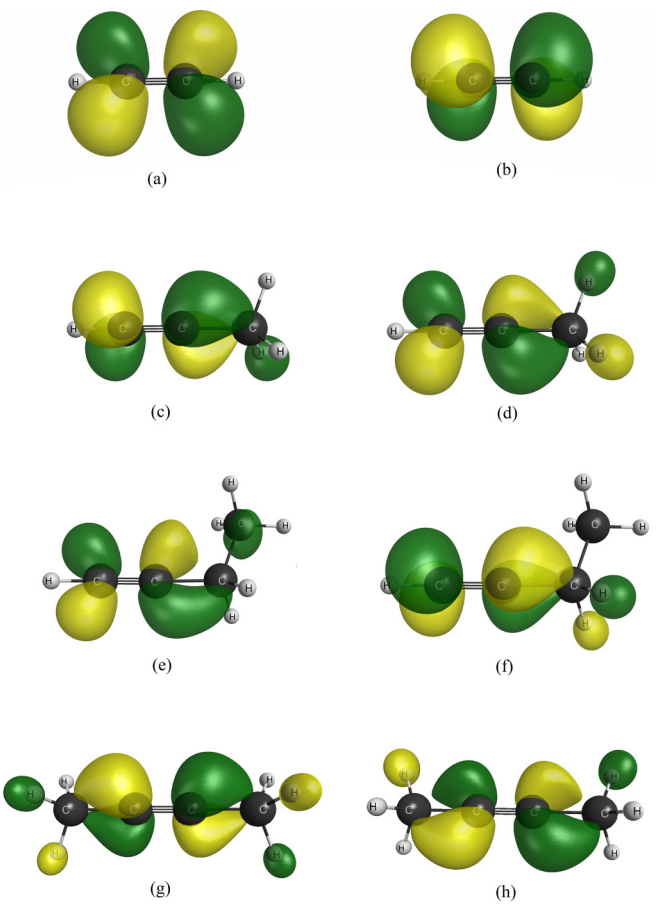

FIG. 15. Resonant orbitals for (a, b) ethyne, (c, d) propyne, (e, f) 1-butyne, and (g, h) 2-butyne. See text for discussion.

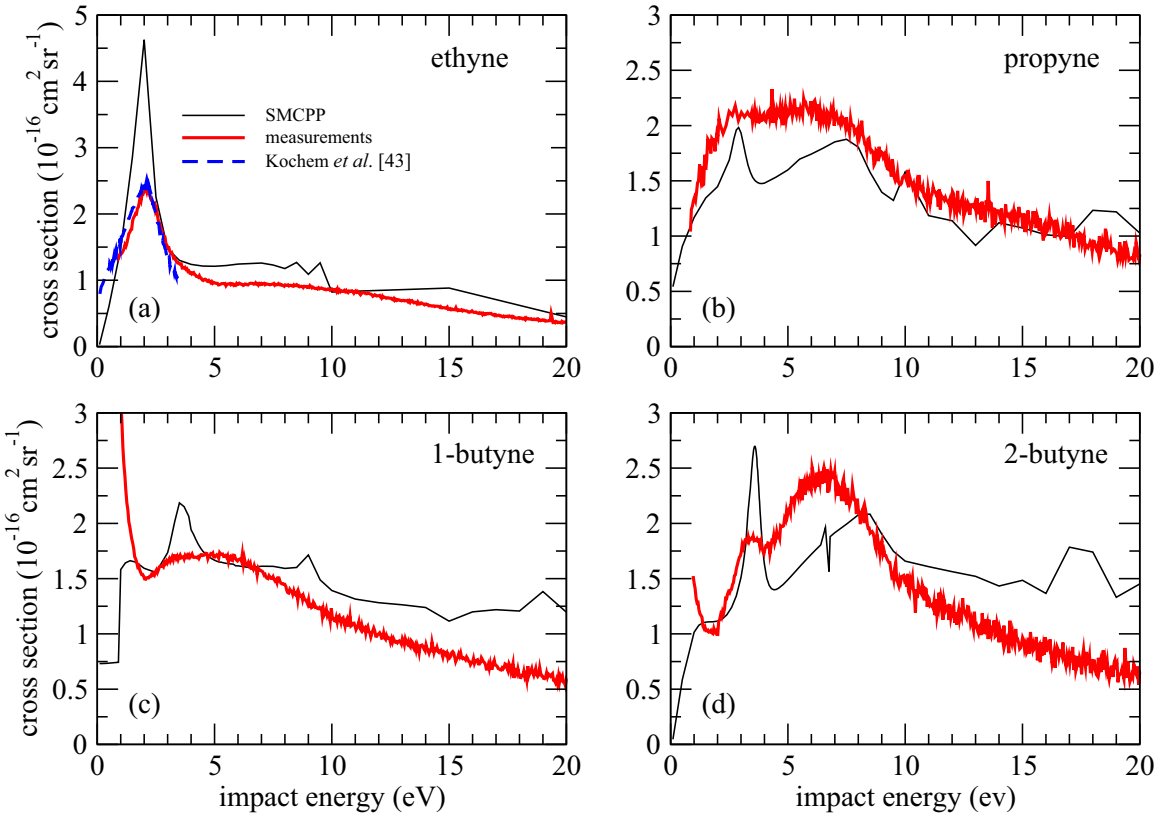

FIG. 16. Differential cross sections for elastic scattering, at a fixed scattering angle of 90°, by (a) ethyne, (b) propyne, (c) 1-butyne, and (d) 2-butyne.

With the methylation of ethyne, replacing a hydrogen atom by a methyl group yielding propyne, the position of the shape resonance moves to higher energy. Our calculation places the π^* resonance at 3.0 eV, whereas the previous TCS measurements place it at 3.4 to 3.6 eV [11,13] and electron energy-loss spectra indicate this resonance at 2.8 and 3.0 eV [45,46]. When analyzing the resonant orbitals, in Figs. 15(c) and 15(d), the contribution of the methyl group is clear. This seems to be the origin of the increase in the resonance energy going from ethyne to propyne. The propyne molecule belongs to the C_{3v} point group but the calculations were performed in the C_s point group, so the degenerate resonant orbital which belongs to the E symmetry of the C_{3v} point group is the combination of the orbitals shown in the Figs. 15(c) and 15(d), which belong to the A' and A'' symmetries of the C_s point group, respectively.

Similarly, 1-butyne can be seen as methylated propyne (or, conversely, ethyne where a hydrogen atom is replaced by an ethyl group). With this change, the LUMO degeneracy is removed, and our calculation indicates, in fact, two shape resonances placed at 3.5 and 3.7 eV, belonging to the A_2 and B_2 symmetries of the C_{2v} symmetry group, respectively. Since these structures are very close in energy they appear in the ICS as a broad structure at around 3.5 eV, at a somewhat higher energy than the 3.2 eV indicated by the TCS [10] and the 2.8 eV obtained earlier by Dance and Walker [45].

Finally, 2-butyne can be seen as an ethyne where the two hydrogen atoms are replaced by methyl groups. In this case, we recover the molecular symmetry and thus the degeneracy of the resonant orbitals. Although 2-butyne belongs to the D_{3h} point group our calculations were performed in the C_{2v} point group, so the degenerate resonant orbital, which belongs to the E'' symmetry of the D_{3h} point group, is the combination of the orbitals shown in Figs. 15(g) and 15(h), which belong to the A_2 and B_2 symmetries of the C_{2v} point group, respectively. Our calculations place the resonance at 3.6 eV, in good agreement with the TCS measurements [12] and earlier electron energy-loss spectra [45]. Overall comparison of our calculated and experimental excitation functions as shown in Fig. 16(d) indicates very good agreement between our calculated and measured resonant positions.

IV. CONCLUSION

We presented calculated and measured elastic electron scattering differential, integral, and momentum transfer cross sections for four alkynes: ethyne, propyne, 1-, and 2-butyne. The experimental measurements in ethyne were carried out in our group earlier [15]. The oscillatory behavior of the DCSs in the resonance energy region (at around 3.0 eV) is clearly dominated by a d-wave pattern, whereas for its methylated derivative, propyne, it displays an f-wave pattern. We observe the DCSs for 1- and 2-butyne to be essentially the same at large scattering angles, but the small dipole polarization of 1-butyne provides for a long-range enhancement of the scattering DCSs at forward scattering angles as can be physically expected. This provides a first test case for two isomers with (1-butyne) and without (2-butyne) dipole moments. The

oscillatory behavior of the DCSs for 1-butyne for lower energies seems also to be dominated by an f-wave pattern.

From the comparison of our ICS with previous TCS data from the literature, we found overall good agreement both in the energy position of the narrow resonance at lower energies (between 2.0 and 4.0 eV) and also in the broad structure at around 7.0–10.0 eV. We also investigated the abrupt drop in the ICS and MTCS for ethyne and 2-butyne as the impact energy goes toward zero. Our calculations revealed that this feature is due to the presence of Ramsauer-Townsend minimum at 0.06 eV and 0.08 eV for ethyne and 2-butyne, respectively.

We found a π^* shape resonance centered at around 2.1, 3.0, and 3.6 eV for ethyne, propyne, and 2-butyne, respectively. In these cases, the resonance is due to electron attachment in the degenerate LUMO. In 1-butyne the degeneracy is removed giving rise to two π^* shape resonances, located at 3.5 and 3.7 eV in our calculations. Due to the proximity in the energy position, the signal of both resonances overlap showing a broader structure at around 3.6 eV.

ACKNOWLEDGMENTS

This research was supported by the Brazilian agencies Conselho Nacional de Desenvolvimento Científico e Tecnológico (CNPq) and Coordenação de Aperfeiçoamento de Pessoal de Nível Superior (CAPES). L.V.S.D., G.M.M., A.S.B., and M.H.F.B. acknowledge computational support from Prof. Carlos Alberto Martins de Carvalho at LFTC-DFIS-UFPR and at LCPAD-UFPR. The work at California State University Fullerton was funded by the US National Science Foundation, Research in an Undergraduate Institution, under Grants No. NSF-RUI AMO 1606905 and No. 1911702 and also by a Fulbright Fellowship to M.Z. The Troy High School students participated in the Troy Tech Summer Internship program.

[1] M. J. Brunger, Int. Rev. Phys. Chem. **36**, 333 (2017).
[2] R. Cortini, M. Barbi, B. R. Caré, C. Lavelle, A. Lesne, J. Mozziconacci, and J.-M. Victor, Rev. Mod. Phys. **88**, 025002 (2016).
[3] A. Feinberg and B. Tycko, Nat. Rev. Cancer. **4**, 143 (2004).
[4] Z. Jin and Y. Liu, Genes & Diseases **5**, 1 (2018).
[5] L. Sanche, Eur. Phys. J. D **35**, 367 (2005).
[6] M. C. A. Lopes, D. G. M. Silva, M. H. F. Bettega, R. F. da Costa, M. A. P. Lima, M. A. Khakoo, C. Winstead, and V. McKoy, J. Phys.: Conf. Ser. **388**, 012014 (2012).
[7] *CRC Handbook of Chemistry and Physics*, 64th ed. *1983-1984*, edited by R. C. Weast, (CRC Press, Boca Raton, FL, 2001), p. E-60.
[8] S. May, S. Karl, O. Božić, in *Proceedings of the 7th European Conference for Aeronautics and Space Sciences* (EUCASS Saïx, France, 2017), pp. 3–6.
[9] S. P. Tarafdar and N. C. Wickramasinghe, Astrophys Space Sci.xs **35**, L41 (1975).
[10] C. Szmytkowski, P. Możejko, M. Zawadzki, K. Maciag, and E. Ptasińska-Denga, Phys. Rev. A **89**, 052702 (2014).
[11] C. Szmytkowski and S. Kwitnewski, J. Phys. B **35**, 3781 (2002).
[12] C. Szmytkowski and S. Kwitnewski, J. Phys. B **36**, 2129 (2003).
[13] C. Makochekanwa, H. Kawate, O. Sueoka, M. Kimura, M. Kitajima, M. Hoshino, and H. Tanaka, Chem. Phys. Lett. **368**, 82 (2003).
[14] Y. Nakano, M. Hoshino, M. Kitajima, H. Tanaka, and M. Kimura, Phys. Rev. A **66**, 032714 (2002).
[15] A. Gauf, C. Navarro, G. Balch, L. R. Hargreaves, M. A. Khakoo, C. Winstead, and V. McKoy, Phys. Rev. A **87**, 012710 (2013).
[16] M. Vinodkumar, A. Barot, and B. Antony, J. Chem. Phys. **136**, 184308 (2012).
[17] A. R. Lopes, M. A. P. Lima, L. G. Ferreira, and M. H. F. Bettega, Phys. Rev. A **69**, 014702 (2004).
[18] A. R. Lopes and M. H. F. Bettega, Phys. Rev. A **67**, 032711 (2003).
[19] S. d'A. Sanchez, A. R. Lopes, M. H. F. Bettega, M. A. P. Lima, and L. G. Ferreira, Phys. Rev. A **71**, 062702 (2005).
[20] M. A. Khakoo, C. E. Beckmann, S. Trajmar, and G. Csanak, J. Phys. B **27**, 3159 (1994).
[21] ARi Industries Inc., Addison, IL 60101 USA, 1HN040B-16.3 biaxial cable.
[22] ETP Equipe Thermodynamique et Plasmas (ETP) model AF151.
[23] J. N. H. Brunt, G. C. King, and F. H. Read, J. Phys. B **10**, 1289 (1977).
[24] M. A. Khakoo, K. Keane, C. Campbell, N. Guzman, and K. Hazlett, J. Phys. B **40**, 3601 (2007).
[25] M. Hughes, Jr., K. E. James, Jr., J. G. Childers, and M. A. Khakoo, Meas. Sci. Technol. **14**, 841 (2003).
[26] R. K. Nesbet, Phys. Rev. A **20**, 58 (1979).
[27] D. F. Register, S. Trajmar, and S. K. Srivastava, Phys. Rev. A **21**, 1134 (1980).
[28] MKS, Granville-Phillips Division, 6450 Dry Creek Parkway, Longmont, CO, 80503 USA.
[29] K. Fedus, C. Navarro, L. R. Hargreaves, and M. A. Khakoo, F. M. Silva and M. H. F. Bettega, C. Winstead, and V. McKoy, Phys. Rev. A **90**, 032708 (2014).
[30] K. Takatsuka and V. McKoy, Phys. Rev. A **24**, 2473 (1981); **30**, 1734 (1984).
[31] M. H. F. Bettega, L. G. Ferreira, and M. A. P. Lima, Phys. Rev. A **47**, 1111 (1993).
[32] G. B. Bachelet, D. R. Hamann, and M. Schlüter, Phys. Rev. B **26**, 4199 (1982).
[33] R. F. da Costa, M. T. N. Varella, M. H. F. Bettega, and M. A. P. Lima, Eur. Phys. J. D **69**, 159 (2015).
[34] G. M. J. Barca, C. Bertoni, L. Carrington, D. Datta, N. De Silva, J. E. Deustua, D. G. Fedorov, J. R. Gour, A. O. Gunina, E. Guidez, T. Harville, S. Irle, J. Ivanic, K. Kowalski, S. S. Leang, H. Li, W. Li, J. J. Lutz, I. Magoulas, J. Mato, V. Mironov, H. Nakata, B. Q. Pham, P. Piecuch, D. Poole, S. R. Pruitt, A. P. Rendell, L. B. Roskop, K. Ruedenberg, T. Sattasathuchana, M. W. Schmidt, J. Shen, L. Slipchenko, M. Sosonkina, V. Sundriyal, A. Tiwari, J. L. Galvez Vallejo, B. Westheimer, M. Wloch, P. Xu, F. Zahariev, and M. S. Gordon, J. Chem. Phys. **152**, 154102 (2020).

[35] A. Sakaamini, B. Hlousek, S. M. Khakoo, M. Zawadzki, M. A. Khakoo, M. B. Kiataki, and M. H. F. Bettega, J. Phys. B **52**, 025206 (2018).
[36] T. H. Dunning, Jr., J. Chem. Phys. **53**, 2823 (1970).
[37] M. H. F. Bettega, C. Winstead, and V. McKoy, Phys. Rev. A **74**, 022711 (2006).
[38] W. J. Hunt and W. A. Goddard III, Chem. Phys. Lett. **3**, 414 (1969).
[39] *CRC Handbook of Chemistry and Physics*, 76th ed., edited by D. R. Lide (CRC Press, Boca Raton, FL, 1995–1996).
[40] E. M. de Oliveira, R. F. da Costa, S. d'A. Sanchez, A. P. P. Natalense, M. H. F. Bettega, M. A. P. Lima, and M. T. N. Varella, Phys. Chem. Chem. Phys. **15**, 1682 (2013).
[41] M. A. Khakoo, H. Silva, J. Muse, M. C. A. Lopes, C. Winstead, and V. McKoy, Phys. Rev. A **78**, 052710 (2008).
[42] S. W. Staley and J. T. Strnad, J. Phys. Chem. **98**, 116 (1994).
[43] K. H. Kochem, W. Sohn, K. Jung, H. Ehrhardt, and E. S. Chang, J. Phys. B **18**, 1253 (1985).
[44] A. Venkatnathan and M. K. Mishrar, Chem. Phys. Lett. **296**, 223 (1998).
[45] D. F. Dance and I. C. Walker, J. Chem. Soc. Faraday Trans. II **70**, 1426 (1974).
[46] C. R. Bowman and W. D. Miller, J. Chem. Phys. **42**, 681 (1965).
[47] B. M. Bode and M. S. Gordon, J. Mol. Graphics Modell. **16**, 133 (1998).